



Comparative Evaluation of Clinical-MRI, Radiomics, and Integrated Nomogram Models for Preoperative Prediction of Placenta Accreta Spectrum

Zhiwei Wang, Xinyao Jiao, Weiwu Liu, Han Song, Jiapeng Li, Jing Hu, Yuanbo Huang, Yang Liu, Sa Huang

Rationale and Objectives: The escalating incidence of placental accreta spectrum (PAS), a pregnancy complication, underscores the need for accurate prenatal diagnosis to guide optimal management strategies. This study aims to develop, validate, and compare various prenatal PAS prediction models integrating clinical data, MRI signs, and radiomics signatures.

Materials and Methods: A cohort comprising 111 patients (72 with PAS and 39 without, denoted as N-PAS) served as the training set, while another 47 patients (33 PAS and 14 N-PAS) constituted the validation set. Clinical features and MRI signs were subjected to univariate and multivariate analyses to construct the Clinical-MRI model. Radiomic features were extracted from MRI images and refined through the Least Absolute Shrinkage and Selection Operator (LASSO) algorithm, thereby establishing the Radiomics model. An optimal set of radiomic features was utilized to derive the Radscore, which was then integrated with clinical features and MRI signs to formulate the Nomogram model. The performance of these models was comprehensively evaluated and compared.

Results: In the validation set evaluation, the Nomogram model, which integrated Radscore, a pivotal clinical indicator, and two MRI signs, demonstrated superior performance. With an area under the curve (AUC) of 0.861 (95% CI: 0.745, 0.978), this model significantly outperformed both the clinical-MRI model (AUC = 0.796, 95% CI: 0.649, 0.943) and the radiomics model (AUC = 0.704, 95% CI: 0.531, 0.877). Specifically, the Nomogram model achieved a high sensitivity of 81.8% and a specificity of 78.6% in the prenatal diagnosis of placenta accreta spectrum (PAS), thereby offering clinicians a precise and efficient diagnostic aid.

Conclusion: The radiomics-derived Radscore serves as an independent predictor for prenatal PAS. Combining Radscore with clinical features and MRI signs into a Nomogram model provides a non-invasive tool with high sensitivity or specificity for PAS diagnosis, enhancing prenatal assessment and management.

Key Words: Magnetic resonance imaging; Placenta accreta spectrum; Radiomics; Nomogram.

© 2024 The Association of University Radiologists. Published by Elsevier Inc. All rights are reserved, including those for text and data mining, AI training, and similar technologies.

Abbreviation: CI confidence intervals, AUC area under the curve, DCA decision curve analysis, LASSO least absolute shrinkage and selection operator, Radscore radiomics score, MRI magnetic resonance imaging, PAS placenta accreta spectrum, PA placenta accreta, PI placenta increta, PP placenta percreta, ROI Region of Interest

Acad Radiol 2025; 32:2041–2052

From the Department of Radiology, The Second Hospital of Jilin University, Changchun 130041, PR China (Z.W., X.J., W.L., H.S., J.L., Y.H., S.H.); Changchun University of Science and Technology, Changchun 130022, Jilin, China (J.H.); Changchun University of Chinese Medicine, Changchun 130117, Jilin, China (Y.L.). Received September 4, 2024; revised October 9, 2024; accepted October 15, 2024. **Address correspondence to:** S.H. e-mail: huangsa@jlu.edu.cn

© 2024 The Association of University Radiologists. Published by Elsevier Inc. All rights are reserved, including those for text and data mining, AI training, and similar technologies.

<https://doi.org/10.1016/j.acra.2024.10.021>

INTRODUCTION

Placenta accreta spectrum (PAS) encompasses a spectrum of pregnancy disorders characterized by the invasion of placental chorionic villous trophoblast cells into the uterine myometrium, stemming from the absence of the basal decidua. This spectrum ranges from placenta accreta (PA), where the invasion is limited, to placenta increta (PI), signifying deeper penetration, and finally placenta percreta (PP), where the invasion transcends the uterine serosa (1,2). Over the past four decades, the global

incidence of PAS has seen a steady increase (3). Consequently, this escalating trend has precipitated a significant surge in case numbers, escalating from a rarity of 1 in 30,000 pregnancies to a concerning frequency of 1 in 300 pregnancies, underscoring the growing prevalence of PAS in obstetric populations (4–6). PAS is a pregnancy complication characterized by abnormal placental attachment, which can cause severe outcomes like postpartum hemorrhage and shock. It may require complex surgeries, including hysterectomy, and can lead to increased maternal health risks and economic burden (7–9). Hence, prenatal assessment for PAS is crucial, as it aids in refining management plans and resource preparedness, ultimately enhancing maternal health outcomes and prognosis.

The prenatal diagnosis of PAS relies on a comprehensive evaluation incorporating various examination modalities. While ultrasound remains a widely used tool, it confronts several limitations: intestinal gas and amniotic fluid can introduce artifacts, significantly impairing diagnostic accuracy, especially when the placenta is located deep within the uterus, such as on the posterior wall. Moreover, the skill level of the operator and limitations in ultrasound visualization can also hinder accurate PAS diagnosis, highlighting key drawbacks of this modality. In contrast, MRI emerges as a superior option for PAS prenatal diagnosis. Being a radiation-free method, MRI is unencumbered by intestinal gas, amniotic fluid, or placental position, offering a larger, clearer, and more three-dimensional field of view. Through multiplanar and multi-sequence imaging, MRI provides a comprehensive depiction of uterine and placental anatomy, enriching the clinical diagnostic picture. Its superior soft tissue resolution and image quality further enhance diagnostic precision. Recent studies have demonstrated that MRI now rivals ultrasound in diagnosing placenta-related morbidities, underscoring its essential role in prenatal evaluation (10,11). The 2018 International Federation of Gynecology and Obstetrics (FIGO) guidelines, along with previous research endeavors, have outlined numerous MRI signs conducive to the diagnosis of PAS (12,13). Although the MRI signs have been endorsed by clinical guidelines, their clinical efficacy is still a matter of debate among prior research. The burgeoning field of radiomics is becoming increasingly prominent in diagnostics, distinguished by its ability to extract high-throughput imaging phenotypes, encompassing morphological attributes, textural nuances, and the distribution of signal intensities. By harnessing the power of radiomics, there is immense potential to significantly enrich the diagnostic process for PAS. It enables the elucidation of a broad spectrum of quantitative placental characteristics from MRI images, thereby providing a wealth of quantitative insights that are crucial for clinical decision-making (14–18).

So far, to our knowledge, various methods have been proposed to predict Placenta Accreta Spectrum (PAS), with varying predictive performances. The aim of this study is to construct multiple predictive models for PAS. By evaluating their diagnostic accuracy, sensitivity, specificity, and the area

under the receiver operating characteristic (ROC) curve, this study aims to determine which model demonstrates the highest performance in prenatal prediction of PAS.

MATERIALS AND METHODS

Patient Population

This retrospective study, approved by the Ethics Committee of our institution, did not require informed consent since it involved no direct interaction with patients or their data collection process. We reviewed medical records spanning from January 2019 to April 2024, identifying 263 patients with suspected PAS based on ultrasound or clinically. Patients were excluded due to incomplete clinical data ($n = 52$), severe MRI artifacts ($n = 23$), early pregnancy ($n = 22$), and multiple pregnancies ($n = 8$). Consequently, a total of 158 patients were included in the training and validation datasets, among which 105 cases were confirmed as PAS through surgery or pathological examination.

Intraoperative and Pathological Criteria for Placental Accreta Spectrum

A comprehensive diagnostic criterion combining clinical surgery with pathology is applied. (1) Non-PAS: The placenta is delivered spontaneously and is intact post-delivery. (2) PAS: Partial placental retention with pathological evidence of abnormal attachment to the myometrium and absence of the basal decidua (PA), or intraoperative identification of placental tissue implanted into the myometrium with difficulty in manual extraction (PI). Additionally, there is substantial hemorrhage or histological findings of placental villi penetrating the myometrium to the serosal layer, and in some cases, the placenta is observed to break through the uterine serosa and potentially involve adjacent organs, with manual removal being impossible (PP).

MRI Imaging Protocol

3.0 T (GE ; General Electric Systems) MRI T2-weighted imaging (T2WI) is acquired using a single-shot fast spin-echo (SSFSE) sequence (TR 2000 ms, TE 100 ms, 384×256 matrix over a field of view of 360×360 mm, 4 mm slice thickness) and 3.0 T (Siemens Medical Systems) MRI were collected through T2-weighted half-fourier acquisition single shot turbo spin echo (HASTE) sequence (TR 2000 ms, TE 87 ms, 256×204.8 matrix over a field of view of 300×300 mm, 4 mm slice thickness) for full placenta coverage in the axial, sagittal and coronal planes.

Clinical Data and MRI Signs Assessment

The clinical data of all patients were retrospectively collected by a radiologist with extensive clinical experience and specialized training, utilizing the hospital's electronic case system. The radiologist rigorously adhered to the predefined

inclusion and exclusion criteria, meticulously screening patients who fulfilled the research requirements, and comprehensively documented the pertinent information of each patient. This encompassed the patient's maternal age, gestational age, gravidity, history of cesarean section, presence of placenta previa, prenatal hemoglobin levels, and platelet counts. Upon completion of data collection, to safeguard the accuracy of the data, we implemented additional quality control measures, involving a second independent radiologist to review the data.

Two additional radiologists, both with 9 years of experience, independently evaluated pelvic MRI images on the Picture Archiving and Communication System (PACS) after reviewing 30 training cases. They were blinded to the patients' prior clinical data, surgical details, and pathology outcomes. Prior to assessing MRI signs, the images were thoroughly examined for artifacts, with those containing significant artifacts being excluded from further evaluation (19). In this study, 11 MRI signs recommended by the 2018 International Federation of Gynecology and Obstetrics (FIGO), the Society of Abdominal Radiology, the European Society of Urogenital Radiology, and previous literature were assessed for their diagnostic utility in PAS. These signs encompassed placental ischemic infarction, dark intraplacental bands on T2WI, abnormal intraplacental vascularity, abnormal vascularization of the placental bed, abnormal vascularization of the uterine serosal surface, myometrial thinning, loss of the retroplacental hypointense line on T2WI, placental/uterine bulge, placental heterogeneity, asymmetric shape of the placenta, and focal exophytic mass (12,13,20). Any discrepancies between the two radiologists' interpretations were resolved by consultation with a senior radiologist who has 22 years of experience in pelvic imaging interpretation, who also provided the final PAS diagnosis. Kappa tests were performed to evaluate the inter-rater agreement on the identification of MRI signs, with a Kappa coefficient greater than 0.75 indicating good agreement. The specific definitions of these 11 MRI signs are detailed in Appendix S1.

Region of Interest (ROI) Delineation and Feature Extraction

MRI images from all eligible patients were retrieved from the Picture Archiving and Communication System (PACS) for the purpose of extracting image features. The delineation of the Region of Interest (ROI) was carried out by two radiologists, each with 9 years of experience, who utilized ITK-snap software (version 3.8.0) to manually segment each slice of the MRI scans, precisely outlining the entire placental ROI. Subsequently, these ROIs were reviewed by a pelvic imaging expert with over 22 years of experience. For radiomic feature extraction, FeAture Explorer Pro (FAE Pro, version 0.5.13) was employed within the Python environment (version 3.7.6). Additionally, to assess inter-observer reproducibility, another radiologist with 8 years of experience blindly segmented 30 randomly selected images. The

inter-observer reproducibility of the extracted features was quantified using intraclass correlation coefficients (ICCs). Figure 1 illustrates the flowchart outlining the participants' selection and the subsequent data processing procedures.

Radiomics Model Construction and Radscore Calculation

Initially, this study extracted a comprehensive dataset containing 1223 high-dimensional radiomic features from the training dataset detailed in Appendix S2, using FAE Pro version 0.5.13 under Python 3.7.6. Subsequently, we identified key radiomic features and utilized them to develop the radiomic model. During the model development process, we employed the Least Absolute Shrinkage and Selection Operator (LASSO) method in R software (version 4.4.0), accompanied by fourteen-fold cross-validation to ensure the model's precision and robustness. After completing the LASSO feature selection, we further conducted a logistic regression analysis to build the radiomics model. After that, we identified radiomic features with a P-value less than 0.01 from all patients' radiomic features through LASSO and logistic regression analysis, and performed normalization and weighting of these features based on their respective coefficients. This process enabled us to calculate an individualized Radscore for each patient. Figure 2 presents the research flowchart, which outlines the methodology and steps involved in our study, from data extraction and feature selection to model construction and Radscore calculation.

Clinical-MRI Model and Nomogram Model Construction

To construct the Clinical-MRI model, we first conducted univariate analysis within the training set, comparing MRI signs and clinical characteristics between the PAS and non-PAS groups. Following this, multivariate logistic regression analysis was employed to identify independent predictors of PAS. Incorporating these independent predictors, we built the Clinical-MRI model within the training set and subsequently tested its performance in the validation set. Additionally, we integrated the Radscore with the optimal MRI signs and clinical variables to develop a nomogram model. This model was grounded in multivariate logistic regression and underwent validation within the validation set. Receiver operating characteristic (ROC) curves were generated to evaluate the discriminatory power of the nomogram model. Calibration curves and the Hosmer-Lemeshow test were utilized to assess the model's goodness-of-fit. Finally, the clinical utility of the nomogram model was examined through decision curve analysis.

Statistical Analysis

Statistical analyses were conducted using IBM SPSS software (version 24.0) and R software (version 4.4.0). The data were classified as continuous variables (presented as mean \pm standard deviation for normally distributed data) and, for non-normally

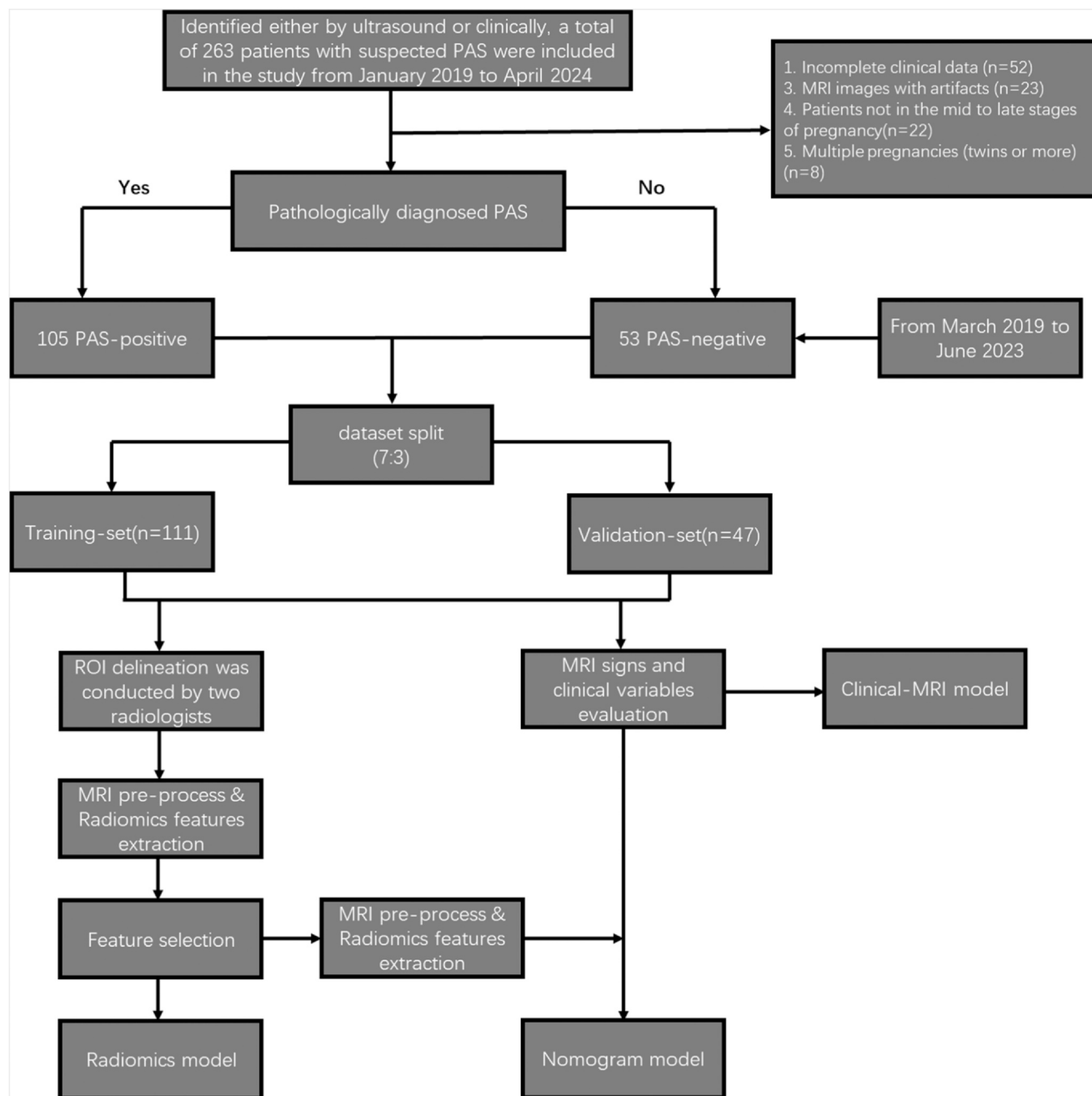


Figure 1. Flowchart of Participants and Data Processing.

distributed data, as median with first and third quartiles (M [Q1, Q3]). Categorical variables were presented as numbers and percentages and analyzed using Student's t test, Mann–Whitney U test, and Chi-square test, respectively. Intraclass correlation coefficients (ICCs) were calculated using R software. The performance of predictive models was assessed using receiver operating characteristic (ROC) curves and the area under the curve (AUC). The DeLong test was utilized to assess differences in ROC curves between models. Results with $P < 0.05$ are considered statistically significant.

RESULTS

Construction, Validation of Clinical-MRI Model

This study included a total of 158 patients with either ultrasound or clinical suspicion of PAS, all of whom were confirmed by surgery or pathology, with 105 cases diagnosed as PAS pregnant women and 53 cases without PAS. Patient characteristics are shown in [Table 1](#). A total of 111 patients were divided into a training set (positive and negative, 72 and 39 respectively) and 47 patients were included in the

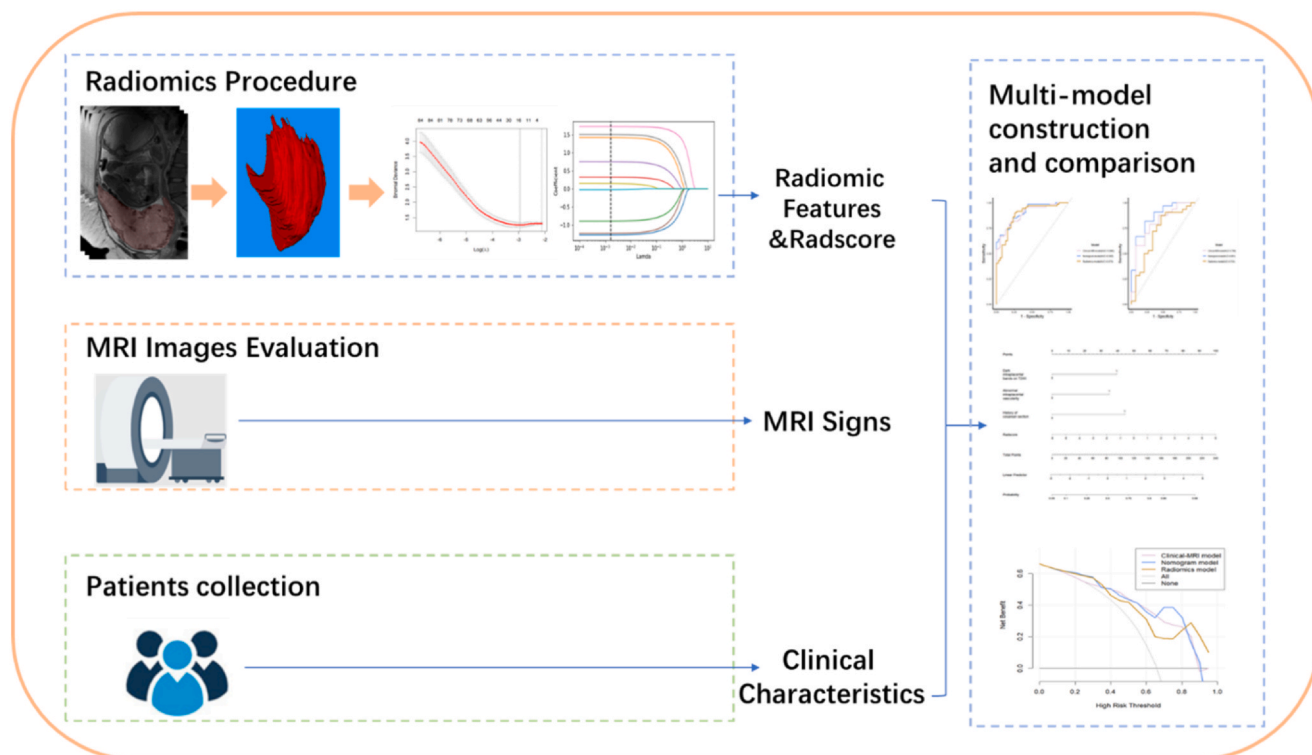


Figure 2. Workflow of our study.

validation set (positive and negative, 33 and 14 respectively). Platelet count (Plt) and gravidity did not conform to a normal distribution and were analyzed using the Mann-Whitney U test for nonparametric comparison. Maternal age, gestational age, and hemoglobin (Hb) conformed to a normal distribution and were analyzed using the one-way ANOVA test. The correlation between Maternal age, Gestational age, and Plt was not significant ($p = 0.223$, $p = 0.106$, $p = 0.811$). History of cesarean section, placenta previa, placental ischemic infarction, dark intraplacental bands on T2WI, abnormal intraplacental vascularity, abnormal vascularization of placental bed, abnormal vascularization of uterine serosal surface, myometrial thinning, loss of retroplacental hypointense line on T2WI, placental/uterine bulge, placental heterogeneity, asymmetric shape of placenta, focal exophytic mass were compared using the chi-square test ($p = 0.000$, 0.924 , 0.002 , 0.000 , 0.000 , 0.683 , 0.297 , 0.463 , 0.489 , 0.375 , 0.392 , 0.051 , 0.037). There were statistically significant differences between the PAS group and the non-PAS group in terms of gravidity, history of cesarean section, Hb, placental ischemic infarction, dark intraplacental bands on T2WI, abnormal intraplacental vascularity and focal exophytic mass ($p < 0.05$). Binary logistic regression analysis was used to determine the independent factors for predicting PAS, and the corresponding regression equation is: $\ln(P/1-P) = 6.35 + 1.77 \times \text{Dark intraplacental bands on T2W images} + 1.82 \times \text{Abnormal intraplacental vascularity} + 1.36 \times \text{History of cesarean section}$. The Clinical-MRI model had an AUC of 0.888 (95%CI: 0.829, 0.947) in the training set and an AUC of 0.796 (95%CI: 0.649, 0.943) in the validation set.

Reproducibility Analysis of Radiomic Features

The overall intraclass correlation coefficient (ICC) for inter-observer reliability was satisfactory, achieving a value of 0.878, reflecting high consistency among observers. Out of all the evaluated features, 1073 demonstrated satisfactory agreement ($\text{ICC} \geq 0.75$), indicating strong reliability. Furthermore, 95 features showed fair agreement ($0.40 \leq \text{ICC} < 0.75$), representing moderate consistency, while 55 features exhibited poor agreement ($\text{ICC} < 0.40$), pointing to low reliability among observers.

Construction, Validation of Radiomics and Nomogram Models

After a series of steps, including ROI delineation and feature extraction, we extracted 1223 features as the foundation for model construction. Utilizing the Least Absolute Shrinkage and Selection Operator (LASSO), we established a radiomics model based on 10 radiomic features through logistic regression modeling. Furthermore, by applying the Least Absolute Shrinkage and Selection Operator (LASSO) and rigorous logistic regression analysis to the radiomic features of all patients, we ultimately identified 3 key radiomic features to calculate the Radscore, with P-values less than 0.01. The Radscore is calculated based on the normalized values and corresponding coefficients of these 3 selected features, ensuring the accuracy and scientific validity of the results. The Radiomics model exhibited an AUC of 0.879 (95% CI: 0.813, 0.946) in the training set and an AUC of 0.704 (95% CI: 0.531, 0.877) in the validation set. Further comparison of

TABLE 1. Clinical Characteristics and MRI Signs of the Training Set and Validation Set

Clinical Variables and MRI Signs	Training Set		Validation Set	
	PAS/N-PAS (72/39)	P-value	PAS/N-PAS (33/14)	P-value
Maternal age (y, $\bar{x} \pm s$)	34.0(29.8,38.2)/ 33.0(28.8,37.0)	0.223	34.0(29.7,38.5)/ 30.9(27.4,34.4)	0.020
Gestational age (w, $\bar{x} \pm s$)	34.9(29.9,39.9)/ 35.6(31.1,40.3)	0.106	34.7(27.8,41.6)/ 32.0(25.0,39.0)	0.045
Gravidity (IQR)	3(1,7)/3(1,6)	0.004	3(1,6)/1(1,3)	0.000
History of cesarean section (%)	61 (84.7)/16(41.0)	0.000	23(69.7)/3(21.4)	0.534
Placenta previa (%)	68 (94.4)/37(94.9)	0.924	32(97.0)/11(78.6)	0.039
Hb (g/L, $\bar{x} \pm s$)	112.2(99.5124.9)/ 117.2(107.4127.0)	0.026	110(98.1121.9)/ 118.0(112.7123.3)	0.025
Plt($10^9/L$,IQR)	200.0(155.0229.0)/ 194.0(169.5228.5)	0.811	195.0(151.5225.0)/ 152.5(128.3217.2)	0.697
Placental ischemic infarction (%)	32(44.4)/6(15.4)	0.002	8(24.2)/5(35.7)	0.421
Dark intraplacental bands on T2WI(%)	46(63.9)/6(15.4)	0.000	22(66.7)/3(21.4)	0.004
Abnormal intraplacental vascularity(%)	45(62.5)/6(15.4)	0.000	15(45.5)/2(14.3)	0.042
Abnormal vascularization of placental bed(%)	38(52.8)/19(48.7)	0.683	14(42.4)/6(42.9)	0.987
Abnormal vascularization of uterine serosal surface(%)	37(51.4)/16(41.0)	0.297	14(42.4)/6(42.9)	0.987
Myometrial thinning(%)	41 (56.9)/25(64.1)	0.463	18(54.5)/11(78.6)	0.037
Loss of retroplacental hypointense line on T2WI(%)	55(76.4)/32(82.1)	0.489	24(72.7)/14(100.0)	0.030
Placental/uterine bulge(%)	34(47.2)/15(38.5)	0.375	19(57.6)/8(57.1)	0.355
Placental heterogeneity(%)	43(59.7)/20(51.3)	0.392	18(54.5)/6(42.9)	0.464
Asymmetric shape of placenta(%)	30(41.7)/10(25.6)	0.051	10(30.3)/5(35.7)	0.716
Focal exophytic mass(%)	17(23.6)/3(7.7)	0.037	27(81.8)/5(35.7)	0.002

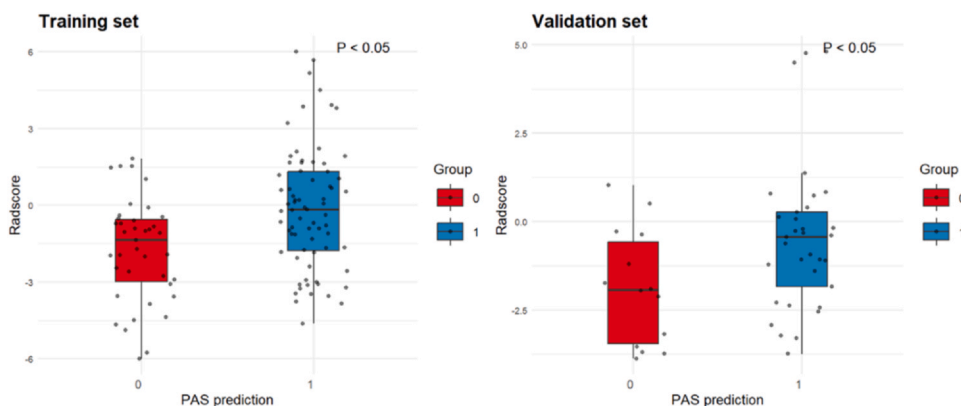


Figure 3. Boxplot of Radscore in PAS group and non-PAS group in training and validation sets.

Radscore between the groups with and without PAS revealed significant differences in both the training and validation sets (Fig 3).

$$\text{Radscore} = -0.191 + 0.0958 \times t2_log\text{-sigma}\cdot 1\text{-mm}\cdot 3D_glszm_Low\text{-GrayLevelZoneEmphasis} + 28.43 \times t2_wavelet\text{-LLH_firstorder_Entropy-}$$

$$0.00485 \times t2_wavelet\text{-LLH_gldm_LargeDependenceLow-GrayLevelEmphasis}$$

Thereafter, a clinical variable with a p-value less than 0.05, along with two MRI signs ("Dark intraplacental bands on T2W images" and "Abnormal intraplacental vascularity", as

TABLE 2. Logistic Regression Model and Nomogram Model

Variables	Clinical-MRI Model			Nomogram Model		
	β	p-value	OR (95%CI)	β	p-value	OR (95%CI)
History of Cesarean sections	1.361	0.030	3.901(1.170,14.171)	1.370	0.033	3.939(1.145,14.818)
Dark intraplacental bands on T2WI	1.773	0.018	5.887(1.432,28.677)	1.542	0.047	4.677(1.073,23.559)
Abnormal intraplacental vascularity	1.818	0.023	6.157(1.372,33.163)	1.740	0.029	5.695(1.262,30.462)
Radscore				0.303	0.041	1.354(1.029,1.858)

detailed in Table 2), were selected and integrated with Radscore to establish a nomogram prediction model (also presented in Table 2). The formula for this model is: $4.83 + 1.54 \times \text{Dark intraplacental bands on T2W images} + 1.74 \times \text{Abnormal intraplacental vascularity} + 1.37 \times \text{History of cesarean section} + 0.30 \times \text{Radscore}$.

The AUC of the nomogram model was 0.902 (95% CI: 0.849, 0.956) in the training set (Fig 4a) and 0.861 (95% CI: 0.745, 0.978) in the validation set (Fig 4b). The model's accuracy, specificity, positive and negative predictive values, and AUC are presented in Table 3. Notably, the nomogram model surpassed the Clinical-MRI model in the validation set ($p = 0.015$); however, it did not significantly differ from the radiomics model in the same set ($P = 0.144$). Although

the radiomics model exhibited high sensitivity (87.5%), its specificity was relatively low (53.3%). Conversely, the Clinical-MRI model had a very high specificity (92.8%) but low sensitivity (57.6%). In contrast, our nomogram model demonstrated a good balance, achieving both high sensitivity (81.8%) and specificity (78.6%) (Tables 3 and 4).

Performance of the Nomogram Model

We have devised a nomogram (Fig 5a) to predict PAS, with its calibration curve showcasing a high congruency between predicted and observed values. The predictive prowess of this nomogram was substantiated by the Hosmer-Lemeshow test, yielding statistically insignificant p-values of 0.396 and 0.197

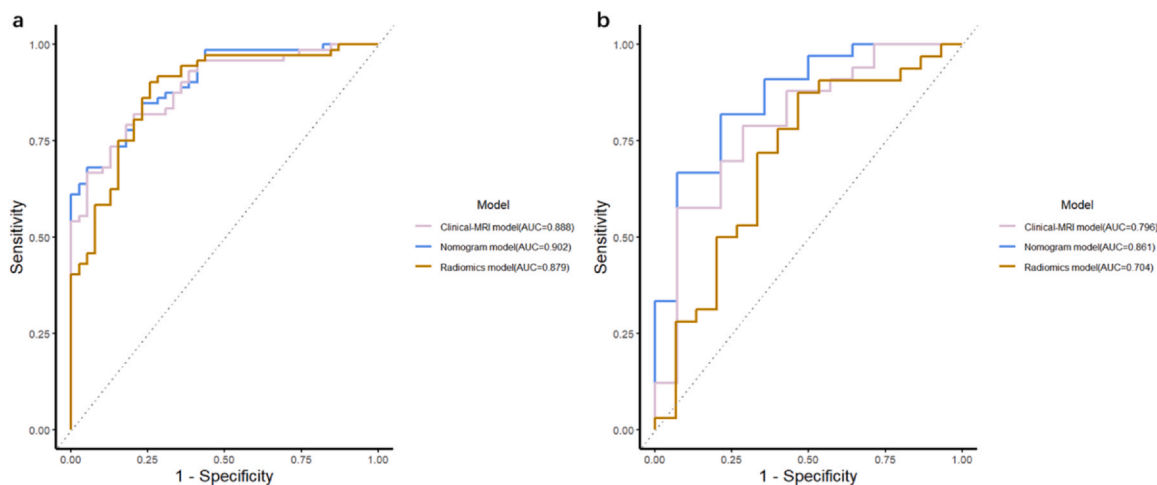


Figure 4. Receiver operating characteristic (ROC) curve of the established three models in the training set (a) and the validation set (b).

TABLE 3. PAS-positive Diagnostic Performance of Three Models in Two Cohort

	AUC (95%CI)	SEN	SPE	ACC	PPV	NPV
Traning set						
Nomogram model	0.902(0.849,0.956)	68.1	94.9	81.1	85.9	72.5
Radiomics model	0.879(0.813,0.946)	90.3	74.4	82.0	82.5	80.6
Clinical-MRI model	0.888(0.829,0.947)	66.7	94.8	77.5	83.1	67.5
Validation set						
Nomogram model	0.861(0.745,0.978)	81.8	78.6	76.6	89.3	57.9
Radiomics model	0.704(0.531,0.877)	87.5	53.3	72.3	80.6	56.2
Clinical-MRI model	0.796(0.649,0.943)	57.6	92.8	74.4	83.8	56.2

TABLE 4. Comparison of the Performance between the Models

Models (AUC)	Training Set (n = 109)	p-value	Validation Set (n = 47)	p-value
Nomogram vs. Clinical-MRI	0.902 vs 0.888	0.206	0.861 VS 0.796	0.015
Radiomics vs. Clinical-MRI	0.879 VS 0.888	0.577	0.704 VS 0.796	0.427
Nomogram vs. Radiomics	0.902 VS 0.879	0.572	0.861 VS 0.704	0.144

in the training and validation sets, respectively (Fig 5b), underscoring its robust performance. Decision curve analysis (DCA) revealed that, compared to the Clinical-MRI model and the radiomics model, our nomogram, which integrates clinical characteristics, MRI signs, and Radscore, showed a

better net benefit (Fig 6). Notably, the composite nomogram model meticulously crafted in this study demonstrated superior predictive performance and enhanced stability in forecasting PAS. Fig. 7a and 7b vividly illustrate the practical application of this nomogram in diagnosing PAS.

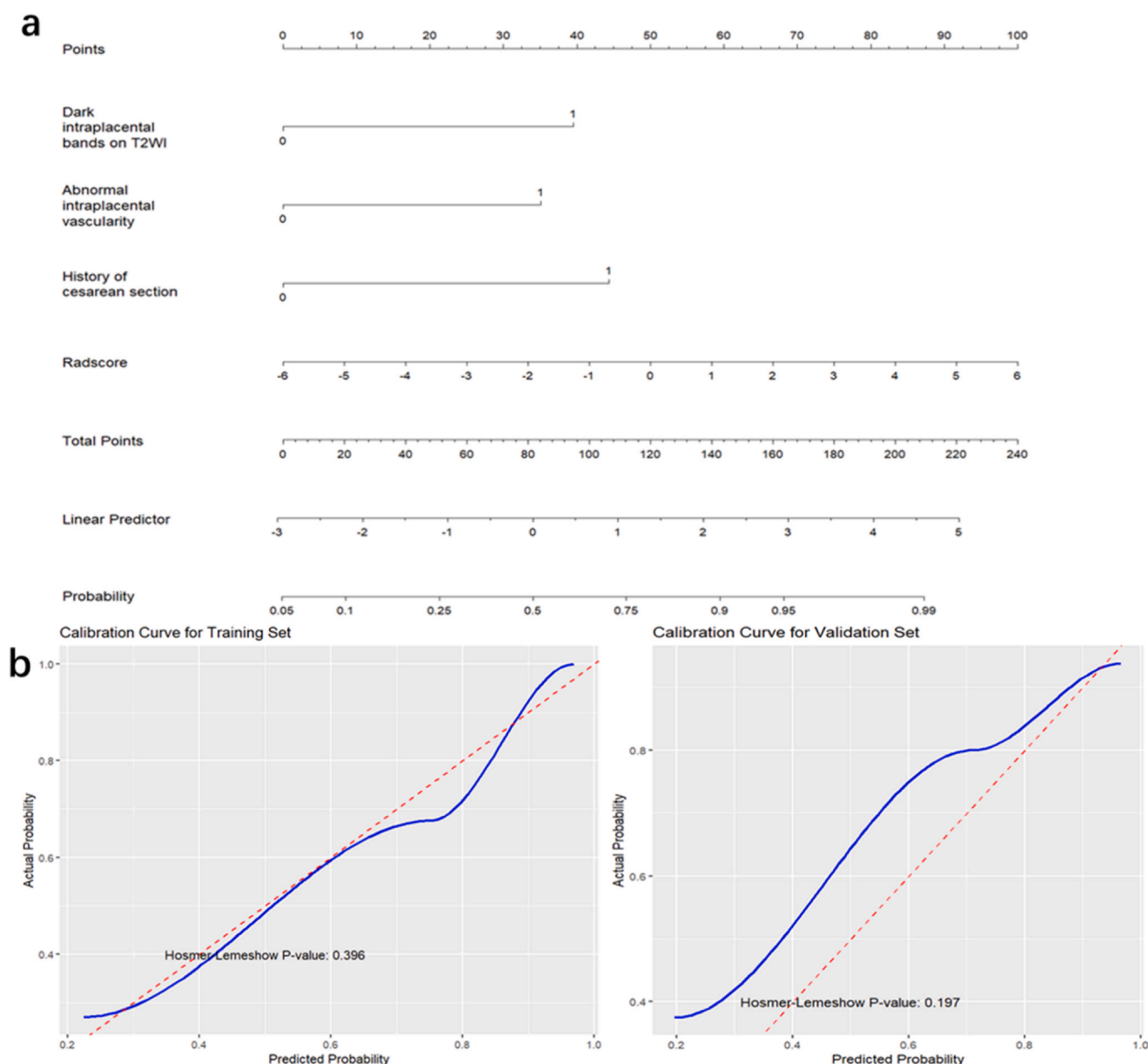


Figure 5. (a) Nomogram model for predicting PAS. **(b)** Calibration curve analysis for the training set and validation set, with p-values calculated by the Hosmer-Lemeshow test also presented in both sets ($p = 0.396$ and 0.197 , respectively).

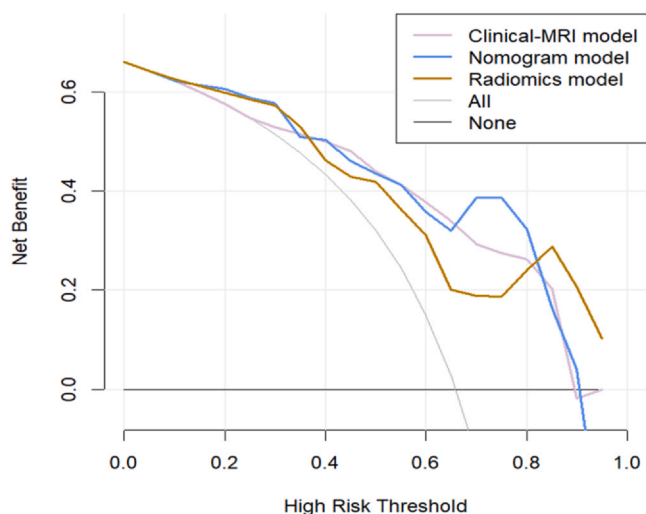


Figure 6. The decision curve analysis conducted within the validation set demonstrates that, across a substantial range of threshold probability intervals, the nomogram model incorporating Radscore outperforms both the Clinical-MRI model and the radiomics model in terms of net benefit. This graphical representation illustrates the relationship between net benefit (y-axis) and the PAS threshold probability (x-axis). The greater the divergence between the model's curve and the reference line, the higher the net benefit achieved.

DISCUSSION

This retrospective study devised three distinct predictive models for prenatal prediction of PAS in the training set: a Clinical-MRI model, a radiomics model, and a nomogram model. The primary objective was to forecast the occurrence of PAS and subsequently evaluate and compare the predictive performance of these models. The Clinical-MRI model combined a single clinical risk factor with two MRI signs. Conversely, the radiomics model extracted and analyzed a total of 1223 quantitative radiomic features to establish its predictive framework. The nomogram model, on the other hand, represented a harmonious integration of a clinical risk factor, two MRI signs, and the quantitative radiomic score (Radscore). In the validation set analysis, the nomogram model exhibited exceptional predictive capabilities, as evidenced by its superior AUC value (0.861, 95% CI: 0.745, 0.948) compared to both the radiomics model (0.704, 95% CI: 0.531, 0.877) and the Clinical-MRI model (0.796, 95% CI: 0.649, 0.943). This robustly substantiates the reliability and effectiveness of the nomogram model in predicting PAS. Notably, the nomogram model achieved a high sensitivity of 81.8%, along with favorable specificity (78.6%) and accuracy (76.6%), providing a robust basis for clinical decision-making. Moreover, the study highlights the unique significance of MRI-based radiomic features, which, translated into Radscore, emerge as an independent predictive factor for positive PAS, paving the way for earlier screening and intervention strategies.

With MRI assuming an increasingly crucial role in the clinical application of PAS, Ueno et al. have pioneered the development of a scoring model that utilizes six distinct MRI signs to predict prenatal PAS, thereby underscoring the enormous potential of

MRI sign-based predictive models in facilitating the diagnosis of PAS (21). However, this model was limited as it was based solely on MRI signs and did not incorporate clinical high-risk factors. In contrast, Xia et al. demonstrated a more comprehensive prenatal predictive potential for PAS by integrating clinical risk factors with MRI signs in their scoring model (20). Li et al. and Huang et al. developed nomogram predictive models that included both clinical high-risk factors and MRI signs, showing good and relatively stable predictive efficacy, yet these models lacked quantitative analysis of MRI images (22,23). In recent years, radiomic models derived from MRI have also been explored for predicting PAS and its related complications. Romeo et al. and Sun et al. constructed models, incorporating 26 and 584 textural features respectively, which demonstrated satisfactory predictive performance (14,15). Our radiomic-based model, after undergoing 14-fold cross-validation and Lasso regression analysis, comprised a 10-feature radiomic model that demonstrated remarkable reproducibility. Subsequently, we meticulously extracted three additional radiomic features with $P < 0.01$ through LASSO and logistic regression analysis of all patients' radiomic features, consisting of one first-order feature and two grayscale texture features. By quantifying these features with radscore and seamlessly integrating them with two MRI signs and one clinical predictor, we forged an integrated nomogram model that is not only clinically practical but also widely applicable. When compared to the nomogram models based solely on MRI signs and clinical risk factors, as reported by Li et al. and Huang et al., our model significantly enhanced diagnostic efficacy, achieving an AUC of 0.861. In our study, the sensitivity of our nomogram model, grounded on radiomic scores, MRI signs, and clinical high-risk factors, stood at 68.1% and 81.8% for the training and validation sets, respectively, while the specificities were 94.9% and 78.6%, respectively. These findings echo the report by Yu et al., who established a predictive model that combines MRI signs with Radscore (24). However, our study broadens the analytical scope by incorporating two MRI signs, one clinical risk factor, and Radscore, thereby encompassing a more exhaustive range of clinical and imaging data. This comprehensive framework offers a holistic approach to PAS risk assessment. The paired Delong test assessment revealed that our nomogram model (AUC = 0.861) outperformed both the radiomic model (AUC = 0.704) and the Clinical-MRI model (AUC = 0.796) in diagnostic efficiency, with significant differences observed between the nomogram and Clinical-MRI models in the validation set ($P < 0.05$).

It is noteworthy that, despite placenta previa and advanced maternal age being identified as key risk factors for PAS in previous studies, our analysis—encompassing both univariate and multivariate logistic regression—failed to uncover a significant association between placenta previa and PAS. Intriguingly, within our training set, we observed a considerable proportion (94.9%) of placenta previa cases in the group without PAS. To safeguard the integrity of our model's construction and performance, we chose to exclude this variable from our modeling process. Furthermore, while myometrial thinning and the loss of the retroplacental hypointense line on

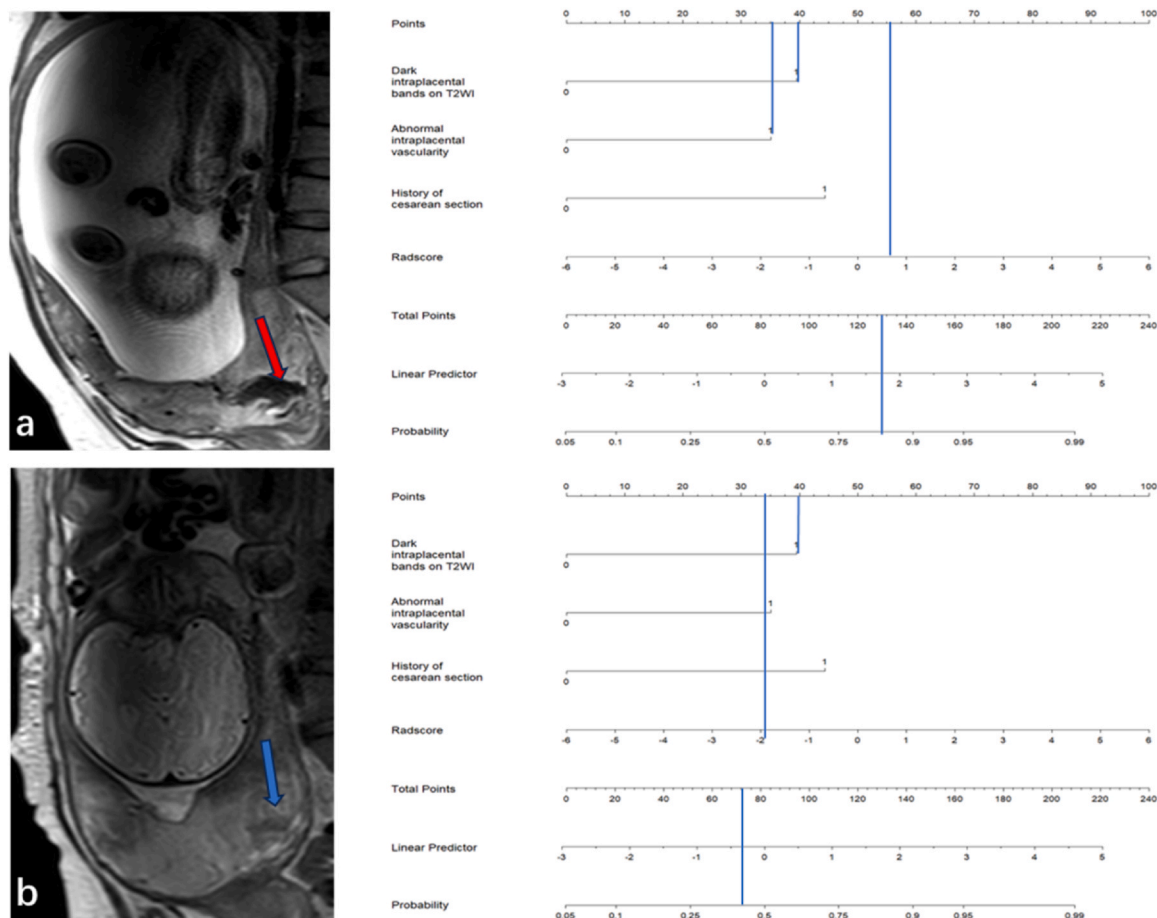


Figure 7. (a) a 34-year-old pregnant woman at 35 weeks of gestation, with no history of cesarean section, presented with MRI signs that included abnormal intraplacental vascularity and dark intraplacental bands on T2WI. The red arrow highlights the abnormal intraplacental vascularity, and the Radscore was 0.74. Using the nomogram, a blue solid line is drawn upwards to determine the points received by each variable; the sum of these points (130) is located on the total points axis. Subsequently, a line is drawn downwards to the probability axis for the presence of PAS, indicating a PAS positivity probability of 85%. Ultimately, the pathological diagnosis for this patient confirmed PAS, aligning perfectly with our prediction derived from the nomogram predictive model, thereby attesting to the model's high degree of accuracy. (b) a 35-year-old pregnant woman at 38 weeks of gestation, also without a history of cesarean section, presented with MRI signs that included dark intraplacental bands on T2WI. The blue arrow points to dark intraplacental bands on T2WI, and the Radscore was -1.97 . Using the nomogram, a blue solid line is drawn upwards to determine the points received by each variable; the sum of these points (74) is located on the total points axis. Then, a line is drawn downwards to the PAS presence probability axis, indicating a PAS positivity probability of 40%. Notably, the intraoperative findings for this patient confirmed the absence of placenta accreta spectrum (PAS), which is in full congruence with our prediction utilizing the nomogram predictive model.

T2WI serve as direct indicators of placental invasion, interpreting these signs in late pregnancy poses challenges due to the natural thinning of the myometrium and the blurring of the hypointense line. Despite their high sensitivity (91%) demonstrated in prior studies, emphasizing their diagnostic significance (25), in our study, these two MRI signs were frequently encountered in the group without PAS, potentially leading to an increased false-positive rate. Additionally, our multifactorial logistic regression analysis failed to show a significant correlation for these MRI signs, which are also heavily dependent on the interpreting radiologist's experience. Lastly, it is worth mentioning that placental asymmetry and placental ischemic infarction exhibited a significant correlation in the univariate analysis ($P < 0.05$); however, this significance did not persist in the multivariate logistic regression analysis. The dark

intraplacental bands observed on T2WI are commonly regarded as a consequence of fibrin deposition, which typically follows placental infarction. These bands are frequently accompanied by abnormal placental vascularity, a phenomenon that may stem from the placenta's increased invasiveness. This heightened invasiveness can lead to vascular remodeling, dilation, localized infarction, and fibrin deposition, all of which are mechanisms the placenta employs to ensure adequate oxygen supply. Consequently, these features demonstrate significant predictive potential for the prenatal diagnosis of PAS (26–28). In our study, we found that clinical characteristics, specifically a history of cesarean section, and two MRI signs—dark intraplacental bands on T2WI and abnormal placental vascularity—were significantly correlated with PAS, as confirmed by surgical and pathological evaluations. Importantly, these factors were

identified as independent predictors for PAS, aligning with previous research findings (29,30).

Our study is not without limitations. Firstly, the relatively small sample size, particularly the paucity of cases with placenta percreta ($n = 5$, accounting for 4.5% in the training set; $N = 3$, 12.3% in the validation set), hinders the establishment of robust radiomic and nomogram models tailored to varying degrees of PAS. Future endeavors should aim to expand the sample size to better predict PAS severity (14). Secondly, despite normalization of MRI images prior to feature extraction, the use of multiple MRI scanners inevitably introduces heterogeneity bias. Thirdly, manual delineation of ROIs by radiologists, though necessary, introduces some subjectivity and variability that could potentially be mitigated through AI-assisted automated segmentation in future studies. Fourthly, we acknowledge that comparing and developing additional machine learning models would further enhance predictive performance for PAS. Lastly, for robust validation and refinement of our predictive models, larger cohorts and multicenter collaborations will be crucial.

In summary, our study demonstrates that the integration of clinical characteristics, key MRI signs, and advanced radiomic features into a nomogram model provides a promising, effective, and reliable diagnostic tool for predicting placenta accreta spectrum (PAS) in clinical settings. This approach has the potential to enhance early detection and facilitate more informed clinical decision-making.

ETHICS APPROVAL AND CONSENT TO PARTICIPATE

This study has received formal approval from the Ethics Review Committee of the Second Hospital of Jilin University. All research procedures were strictly conducted in accordance with the principles outlined in the Declaration of Helsinki (1964 and its subsequent amendments). Given the retrospective nature of this study, which does not directly involve current medical interventions or additional information collection from patients, the Ethics Committee has granted an exemption from the requirement for written informed consent from the subjects. Nevertheless, during the process of data processing and analysis, we have strictly adhered to relevant laws and regulations regarding data protection and personal privacy, ensuring that all information remains anonymous while its confidentiality is fully preserved. We solemnly commit that this study will not involve any actions that may infringe upon the rights and interests of the subjects or divulge their personal information.

AUTHOR CONTRIBUTIONS

ZW, XJ and SH conceived the idea for the article. ZW drafted the manuscript. WL, HS, JL and YH were responsible for data collection. ZW and XJ were responsible for data analysis. JH and YL reviewed and edited the final

version of the manuscript. All authors contributed substantially to the preparation of the manuscript.

FUNDING

This research is supported by the Science and Technology Development Program of Jilin Province, China (No. 20230204112YY).

DECLARATION OF COMPETING INTEREST

The authors declare that they have no known competing financial interests or personal relationships that could have appeared to influence the work reported in this paper.

ACKNOWLEDGMENTS

None declared.

CONSENT FOR PUBLICATION

The manuscript obtained consent for publication from all the authors.

APPENDIX A. SUPPORTING INFORMATION

Supplemental data associated with this article can be found in the online version at [doi:10.1016/j.acra.2024.10.021](https://doi.org/10.1016/j.acra.2024.10.021).

REFERENCES

1. Silver RM, Barbour KD. Placenta accreta spectrum: accreta, increta, and percreta. *Obstet Gynecol Clin North Am* 2015; 42(2):381–402.
2. Jauniaux E, Ayres-de-Campos D, Langhoff-Roos J, Fox KA, Collins S. FIGO classification for the clinical diagnosis of placenta accreta spectrum disorders. *Int J Gynaecol Obstet* 2019; 146(1):20–24.
3. Jauniaux E, Hussein AM, Fox KA, Collins SL. New evidence-based diagnostic and management strategies for placenta accreta spectrum disorders. *Best Pract Res Clin Obstet Gynaecol* 2019; 61:75–88.
4. Jauniaux E, Chantraine F, Silver RM, Langhoff-Roos J. FIGO consensus guidelines on placenta accreta spectrum disorders: epidemiology. *Int J Gynaecol Obstet* 2018; 140(3):265–273.
5. Jauniaux E, Bunce C, Gronbeck L, Langhoff-Roos J. Prevalence and main outcomes of placenta accreta spectrum: a systematic review and meta-analysis. *Am J Obstet Gynecol* 2019; 221(3):208–218.
6. Khong TY. The pathology of placenta accreta, a worldwide epidemic. *J Clin Pathol* 2008; 61(12):1243–1246.
7. Li P, Tang Y, Jiang Y, Li D. Analysis of clinical features of 231 cases with pernicious placenta previa: a retrospective cohort study. *Medicine (Baltimore)* 2021; 100(11):e25023.
8. Jauniaux E, Bhide A. Prenatal ultrasound diagnosis and outcome of placenta previa accreta after cesarean delivery: a systematic review and meta-analysis. *Am J Obstet Gynecol* 2017; 217(1):27–36.
9. Chu C, Liu M, Zhang Y, et al. Quantifying magnetic resonance imaging features to classify placenta accreta spectrum (PAS) in high-risk gravid patients. *Clin Imaging* 2021; 80:50–57.
10. D'Antonio F, Iacovella C, Bhide A. Prenatal identification of invasive placentation using ultrasound: systematic review and meta-analysis. *Ultrasound Obstet Gynecol* 2013; 42(5):509–517.

11. Familiari A, Liberati M, Lim P, et al. Diagnostic accuracy of magnetic resonance imaging in detecting the severity of abnormal invasive placenta: a systematic review and meta-analysis. *Acta Obstet Gynecol Scand* 2018; 97(5):507–520.
12. Patel-Lippmann KK, Planzand VB, Phillips CH, et al. Placenta accreta spectrum disorders: update and pictorial review of the SAR-ESUR joint consensus statement for MRI. *Radiographics* 2023; 43(5):e220090.
13. Jha P, Pöder L, Bourgioti C, et al. Society of abdominal radiology (SAR) and European Society of Urogenital Radiology (ESUR) joint consensus statement for MR imaging of placenta accreta spectrum disorders. *Eur Radiol* 2020; 30(5):2604–2615.
14. Romeo V, Ricciardi C, Cuocolo R, et al. Machine learning analysis of MRI-derived texture features to predict placenta accreta spectrum in patients with placenta previa. *Magn Reson Imaging* 2019; 64:71–76.
15. Sun H, Qu H, Chen L, et al. Identification of suspicious invasive placenta based on clinical MRI data using textural features and automated machine learning. *Eur Radiol* 2019; 29(11):6152–6162.
16. Wu Q, Yao K, Liu Z, et al. Radiomics analysis of placenta on T2WI facilitates prediction of postpartum haemorrhage: a multicentre study. *EBioMedicine* 2019; 50:355–365.
17. Do QN, Lewis MA, Xi Y, et al. MRI of the placenta accreta spectrum (PAS) disorder: radiomics analysis correlates with surgical and pathological outcome. *J Magn Reson Imaging* 2020; 51(3):936–946.
18. Chen E, Mar WA, Horowitz JM, et al. Texture analysis of placental MRI: can it aid in the prenatal diagnosis of placenta accreta spectrum? *Abdom Radiol (NY)* 2019; 44(9):3175–3184.
19. Lane BF, Vandermeer FQ, Oz RC, et al. Comparison of sagittal T2-weighted BLADE and fast spin-echo MRI of the female pelvis for motion artifact and lesion detection. *AJR Am J Roentgenol* 2011; 197(2):W307–W313.
20. Xia J, Hu Y, Huang Z, et al. A novel MRI-based diagnostic model for predicting placenta accreta spectrum. *Magn Reson Imaging* 2024; 109:34–41.
21. Ueno Y, Maeda T, Tanaka U, et al. Evaluation of interobserver variability and diagnostic performance of developed MRI-based radiological scoring system for invasive placenta previa. *J Magn Reson Imaging* 2016; 44(3):573–583.
22. Huang F, Lyu GR, Lai QQ, Li YZ. Nomogram model for predicting invasive placenta in patients with placenta previa: integrating MRI findings and clinical characteristics. *Sci Rep* 2024; 14(1):200.
23. Li Q, Zhou H, Zhou K, et al. Development and validation of a magnetic resonance imaging-based nomogram for predicting invasive forms of placental accreta spectrum disorders. *J Obstet Gynaecol Res* 2021; 47(10):3488–3497.
24. Yu H, Yin H, Zhang H, et al. Placental T2WI MRI-based radiomics-clinical nomogram predicts suspicious placenta accreta spectrum in patients with placenta previa. *BMC Med Imaging* 2024; 24(1):146.
25. Alamo L, Anaye A, Rey J, et al. Detection of suspected placental invasion by MRI: do the results depend on observer experience? *Eur J Radiol* 2013; 82(2):e51–e57.
26. Baughman WC, Corteville JE, Shah RR. Placenta accreta: spectrum of US and MR imaging findings. *Radiographics* 2008; 28(7):1905–1916.
27. Derman AY, Nikac V, Haberman S, et al. MRI of placenta accreta: a new imaging perspective. *AJR Am J Roentgenol* 2011; 197(6):1514–1521.
28. Hou S, Song Y, Wu J, et al. Comparison of magnetic resonance imaging of the lower uterine segment in pregnant women with central placenta previa with and without placenta accreta spectrum from a single center. *Med Sci Monit* 2021; 27:e932759.
29. Romeo V, Sarno L, Volpe A, et al. US and MR imaging findings to detect placental adhesion spectrum (PAS) in patients with placenta previa: a comparative systematic study. *Abdom Radiol (NY)* 2019; 44(10):3398–3407.
30. Romeo V, Verda F, Sarno L, et al. Prediction of placenta accreta spectrum in patients with placenta previa using clinical risk factors, ultrasound and magnetic resonance imaging findings. *Radiol Med* 2021; 126(9):1216–1225.